Chapter 7
Orbital Rule for Electron Transport of Molecular Junctions

Tomofumi Tada

Abstract Constructive and destructive interference are typical features of electron transport in molecular junctions, which appear as parabolic curves and sharp dips of transmission functions, respectively. To understand the quantum interference properties in molecular junctions, the Green's function method with tight-binding models was adopted, and the quantum interference was analyzed in terms of orbitals, which leads to an efficient *orbital rule* for qualitative predictions of electron transport in molecular junctions. A minimum model, a two-site tight-binding model, was used to explain the *orbital rule* for electron transport without ambiguity. The orbital bases in tight-binding models are typically atomic orbitals, and thus the tight-binding model can be easily extended to larger molecules by simply adding atomic sites. As the next example, a three-site triangular tight-binding model was introduced. The quantum interference that appears in the three-site model can be easily understood using the *orbital rule*. With regard to the orbital bases as molecular orbitals, the triangular tight-binding model could efficiently explain the destructive interference recently observed in a large molecular unit. In the final part, we also examine the applicability of the *orbital rule* for molecular spin systems including spin-flip processes.

Keywords Electron transport • Green's function • Tight-binding model • Orbital rule

7.1 Introduction

Quantum interference that appears as the result of superposition between possible electronic propagations is a typical phenomenon in quantum mechanics. The simplest picture of quantum interference can be explained with the concept of path-interference. Let us assume that only the left- and right-pathways are allowed for conduction electrons in the ring system shown in Fig. 7.1. When the difference of the transport distance between the two pathways is an integral multiple of the

T. Tada (✉)

Materials Research Center for Element Strategy, Tokyo Institute of Technology, Tokyo, Japan
e-mail: tada.t.ae@m.titech.ac.jp

Fig. 7.1 Schematic of two different electron pathways in a ring-shaped apparatus. We can easily expect that no interactions occur between the two propagating states at *dotted mid-points* in a large ring, but such interaction will appear in molecular-sized rings

Left-way

∼1 μm

Right-way
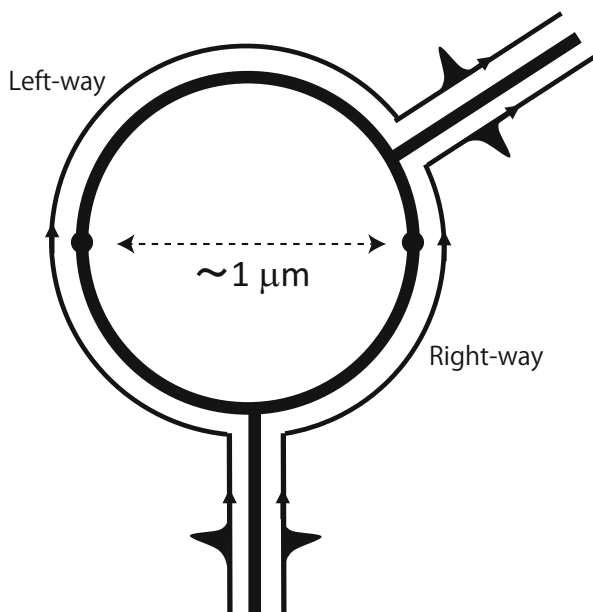
wavelength of conduction electrons, the two propagation states are superposed in a constructive manner, whereas when half of the wavelength remains in the distance difference, the two propagation states are superposed in a destructive manner. It is well known that quantum interference is a key in the quantum physics of the Aharonov-Bohm (AB) effect [1, 2], and the AB-ring is a very efficient apparatus for quantum physics. This explanation assumes that the two electron pathways are absolutely distinct; therefore, the size of the ring must be sufficiently large to avoid unexpected interactions[1] between the two propagations at mid-points (e.g., dotted points in Fig. 7.1). However, what happens when the macroscopic size of the ring is decreased to a molecular size? In molecular rings, the assumption (i.e., no interactions between the two propagations at mid-points) will be broken. Thereby, the emergence of quantum interference in molecular rings as a result of path interference may become ambiguous.

Theoretical investigations on the quantum interference effect in molecular junctions began from 1988 to the early 2000s [3–6], mainly with the use of ring-shaped molecules. The first report on the quantum interference effect in molecular junctions by Sautet and Joachim was based on the benzene molecule [3], and the constructive or destructive interference in electron transport via the benzene ring was obtained

---

[1]The so-called *measurement problem* in quantum mechanics is still not resolved; therefore, we cannot deny the presence of any suspicious interactions between two propagating states that are separated by large distances. The term *interaction* used in this chapter denotes an apparent interaction that is explicitly represented in Hamiltonian.
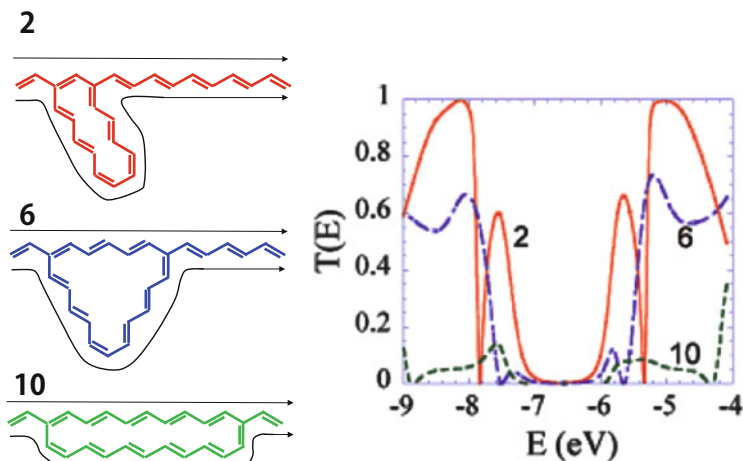
Fig. 7.2 Carbon molecular junctions theoretically investigated and the calculated transmission functions by Baer and Neuhauser (Reprinted with permission from Ref. [6]. Copyright 2002 American Chemical Society)

using scattering state theory. In addition, the model junctions introduced by Baer and Neuhauser [6] were probably designed for investigation of the quantum interference effect in molecular junctions along the concept of path-interference. Figure 7.2 shows their molecular junctions and calculated transmission functions in which parabolic curves and abrupt drops of transmission functions appear depending of the junction structures and energy of the transmitted electrons. However, quantum interference was also confirmed in larger complicated molecules where the electron pathways cannot be identified. To understand the quantum interference in molecular junctions, the concept of interorbital interference rather than path-interference was proposed based on the Green's function approach [7]. According to interorbital interference, the key quantity of the quantum interference in molecular junctions is not the distance differences but the orbital-phase differences between connection points.

7.2   Tight-Binding Model for Molecular Junctions

In this section, the Green's function method based on a single-orbital per single-site model, the simplest tight-binding (TB) model, is introduced, and an orbital-phase rule to achieve a qualitative understanding of electron transport in single molecular junctions is explained. The model corresponds to the Hückel approximation when a single orbital is regarded as a π atomic orbital (AO) in a planar molecule composed of carbon atoms. The simplest TB model can also be useful for more general systems by considering that the base of the single orbital is given in the molecular orbital

(MO) space or in the AO-and-spin direct product space, as shown in the latter part of this section. Here, a qualitative relationship between orbitals and quantum transport is explained as a result of constructive or destructive interference, regardless of the base type for the orbitals.

Quantum interference is typically understood in terms of phase-related matters, and thus the interference effect may not be expected to appear in a phase-broken process (i.e., incoherent transport). However, a similar quantum interference effect can appear even for spin-dependent transport including spin-flip processes (i.e., incoherent transport). The key factor that leads to the quantum interference effects in many different cases is the similarity of the matrix form used to represent the junctions.

For electrodes, a one-dimensional (1D) metallic chain is adopted for simplicity. The base adopted for the orbitals of 1D electrodes does not have any limitations, that is, AO, MO, spin-spin direct product, etc. are acceptable, depending on the orbital base of the system sandwiched between the electrodes. It is also assumed that the interaction between the sandwiched system and the left/right 1D electrode is represented by a single hopping parameter (Fig. 7.3). Although these conditions are extensively simplified compared with the realistic conditions for nanojunctions, they are rather efficient for the derivation of a qualitative relationship between orbitals and conductance.
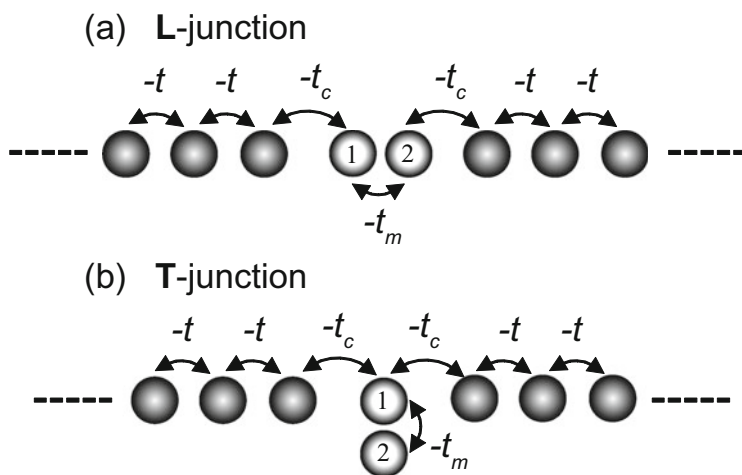

Fig. 7.3 1D tight-binding molecular junctions for the two-site model. The sandwiched diatomic molecule is composed of atoms 1 and 2. We adopted the nearest-neighbor hopping; $-t$ in the electrode, $-t_c$ for electrode-molecule hopping, and $-t_m$ for intramolecular hopping parameters. Atoms 1 and 2 are respectively connected to the left- and right-electrodes in (**a**) a L-junction (Line-contact), and atom 1 is only connected to both electrodes in (**b**) a T-junction (T-shaped contact)

Let us start from the matrix representation of the 1D tight-binding model. The Hamiltonian of the system can be represented as

$$
\mathbf{H} = \left(\begin{array}{c|c|c} \mathbf{H_L} & \mathbf{t_L^\dagger} & \mathbf{0} \\ \hline \mathbf{t_L} & \mathbf{H_M} & \mathbf{t_R^\dagger} \\ \hline \mathbf{0} & \mathbf{t_R} & \mathbf{H_R} \end{array} \right),
\tag{7.1}
$$

where $\mathbf{H_M}$ represents the Hamiltonian of a sandwiched molecule and the Hamiltonian matrices $\mathbf{H_L}$ and $\mathbf{H_R}$ for the electrodes are shown as

$$
\mathbf{H_L} = \begin{array}{c} \\ \vdots \\ m{-}4 \\ m{-}3 \\ m{-}2 \\ m{-}1 \end{array} \begin{array}{cccc} \cdots \quad m{-}4 \quad m{-}3 \quad m{-}2 \quad m{-}1 \\ \left(\begin{array}{ccccc} \ddots & \ddots & \ddots & \ddots \\ \ddots & \varepsilon_0 & -t & 0 & 0 \\ \ddots & -t & \varepsilon_0 & -t & 0 \\ \ddots & 0 & -t & \varepsilon_0 & -t \\ & 0 & 0 & -t & \varepsilon_0 \end{array} \right) \end{array},
\tag{7.2}
$$

$$
\mathbf{H_R} = \begin{array}{c} n{+}1 \\ n{+}2 \\ n{+}3 \\ n{+}4 \\ \vdots \end{array} \begin{array}{c} n{+}1 \quad n{+}2 \quad n{+}3 \quad n{+}4 \quad \cdots \\ \left(\begin{array}{ccccc} \varepsilon_0 & -t & 0 & 0 \\ -t & \varepsilon_0 & -t & 0 & \ddots \\ 0 & -t & \varepsilon_0 & -t & \ddots \\ 0 & 0 & -t & \varepsilon_0 & \ddots \\ & \ddots & \ddots & \ddots & \ddots \end{array} \right) \end{array},
\tag{7.3}
$$

$$
\mathbf{t_L} = \begin{array}{c} m \\ m{+}1 \\ m{+}2 \\ \vdots \end{array} \begin{array}{c} \cdots \quad m{-}3 \quad m{-}2 \quad m{-}1 \\ \left(\begin{array}{cccc} \cdots & 0 & 0 & -t \\ & & 0 & 0 \\ & & & 0 \\ & & \vdots & \vdots \end{array} \right) \end{array},
\tag{7.4}
$$

and

$$
\mathbf{t_R} = \begin{array}{c} \\ n+1 \\ n+2 \\ n+3 \\ \vdots \end{array} \begin{array}{ccccc} \cdots & n-2 & n-1 & n \\ \begin{pmatrix} \cdots & 0 & 0 & -t \\ & & 0 & 0 \\ & & & 0 \\ & & & \vdots \end{pmatrix} \end{array}, \tag{7.5}
$$

where the base index of $\mathbf{H_M}$ is running from m to n (i.e., the matrix size of $\mathbf{H_s}$ is $n-m+1$). For the coupling matrices, $\mathbf{t_L}$ and $\mathbf{t_R}$ in Eqs. 7.4 and 7.5, it was assumed that the atoms connecting with the left and right electrodes are different, and the matrix indices for the two atoms are defined as m and n in $\mathbf{H_M}$. When the atoms connecting with the left and right electrodes are identical (i.e., the index is m in $\mathbf{H_M}$), the coupling matrix $\mathbf{t_R}$ is changed as

$$
\mathbf{t_R} = \begin{array}{c} \\ n+1 \\ n+2 \\ n+3 \\ \vdots \end{array} \begin{array}{cccc} m & m+1 & \cdots & n \\ \begin{pmatrix} -t & 0 & \cdots & 0 \\ 0 & 0 & \cdots & 0 \\ 0 & & & 0 \\ \vdots & & & \vdots \end{pmatrix} \end{array}, \tag{7.6}
$$

Note that the matrix forms of $\mathbf{H_M}$ are dependent on the sandwiched molecule. Examples for the matrices are given in the following sections.

7.2.1 Two-Site Model

A two-site TB model (i.e., diatomic molecule) connected to 1D electrodes is introduced first. Figure 7.3 shows two typical contact structures (i.e., L- and T-junctions) in the two-site TB model. The matrix elements for the two contact models are given as

$$
\mathbf{H^L} = \begin{array}{c} \\ \vdots \\ \\ \\ 1 \\ 2 \\ \\ \\ \vdots \end{array} \begin{array}{ccccccc} & & & 1 & 2 & & \cdots \\ \begin{pmatrix} \ddots & \ddots & & & & & \\ \ddots & \varepsilon_0 & -t & & & & \\ & -t & \varepsilon_0 & -t_c & & & \\ & & -t_c & \varepsilon_\alpha & -t_m & & \\ & & & -t_m & \varepsilon_\alpha & -t_c & \\ & & & & -t_c & \varepsilon_0 & -t \\ & & & & & -t & \varepsilon_0 & \ddots \\ & & & & & & \ddots & \ddots \end{pmatrix} \end{array}, \tag{7.7}
$$

and

$$
\mathbf{H^T} = \begin{array}{c} \\ \\ \\ 1 \\ 2 \\ \\ \\ \\ \end{array}
\begin{pmatrix}
\ddots & \ddots & & & & & \\
\ddots & \varepsilon_0 & -t & & & & \\
 & -t & \varepsilon_0 & -t_c & & & \\
 & & -t_c & \varepsilon_\alpha & -t_m & -t_c & \\
 & & & -t_m & \varepsilon_\alpha & 0 & \\
 & & & -t_c & 0 & \varepsilon_0 & -t \\
 & & & & & -t & \varepsilon_0 & \ddots \\
 & & & & & & \ddots & \ddots
\end{pmatrix}, \qquad (7.8)
$$

where the base indices of $\mathbf{H_s}$ are 1 and 2, and ε_0 and ε_α are the on-site energies of atoms in the electrodes and in the molecule, respectively. The hopping parameters, $-t_m$ and $-t_c$, correspond to those for the sandwiched molecule itself and molecule-electrode coupling, respectively.

In the non-equilibrium Green's function method for electron transport [8], the transmission probability T, which is related to conductance as $G = 2e^2/h$ in Landauer's formula [9], is expressed with the advanced/retarded Green's functions, $\mathbf{G}^{A/R}$ of the molecule and the local density of states ρ of the apex atom in each electrode, as follows [10]:

$$
T_{rs}(E) = \frac{(2\pi t_c^2)^2}{2} G_{sr}^A(E) G_{rs}^R(E) \rho(E) \rho(E). \qquad (7.9)
$$

The orbital index r/s corresponds to the AO connected to the left-/right-electrode. $G^{A/R}(E)$ is the advanced/retarded Green's function $\mathbf{G}^{A/R}(E)$, which is represented as $\mathbf{G}^{A/R}(E) = [E\mathbf{1} - \mathbf{H}_{\text{mol}} - \Sigma_L^{A/R} - \Sigma_R^{A/R}]^{-1}$, where $\mathbf{H}_{\text{mol}}$ is the 2×2 Hamiltonian matrix in the basis of AOs in the two-site models, and $\Sigma_{L/R}$ is the 2×2 self-energy matrix of the left-/right-electrode. The interaction between the sandwiched molecule and each electrode is represented with a single hopping parameter t_c so that only a single element takes a non-zero value in the 2×2 self-energy matrix (e.g., $(\Sigma_L)_{i,j} = t_c^2 g_{\text{elec}}\delta_{ij}\delta_{i1}$ and $(\Sigma_R)_{i,j} = t_c^2 g_{\text{elec}}\delta_{ij}\delta_{i2}$ for the Line-contact, where g_{elec} is the Green's function for the electrodes). The transmission probability in the matrix-based Green's function for electron transport is generally represented as $T(E) = \text{Tr}[i\{\Sigma_L^R(E) - \Sigma_L^A(E)\}\mathbf{G}^R(E)i\{\Sigma_R^R(E) - \Sigma_R^A(E)\}\mathbf{G}^A(E)]$ [8]. Using the matrix elements for the two-site TB model, the expression of $T(E)$ shown in Eq. 7.9 is easily obtained.

Figure 7.4 shows the calculated transmission probabilities for L- and T-junctions. In both cases, the transmission probabilities have sharp peaks at energies of $-0.5t$ and $0.5t$, which are the orbital levels of the highest occupied MO (HOMO) $-0.5t$, and lowest unoccupied MO (LUMO) $0.5t$, of the diatomic molecule. However, at the mid-gap between the HOMO and LUMO, the two contacts show a clear
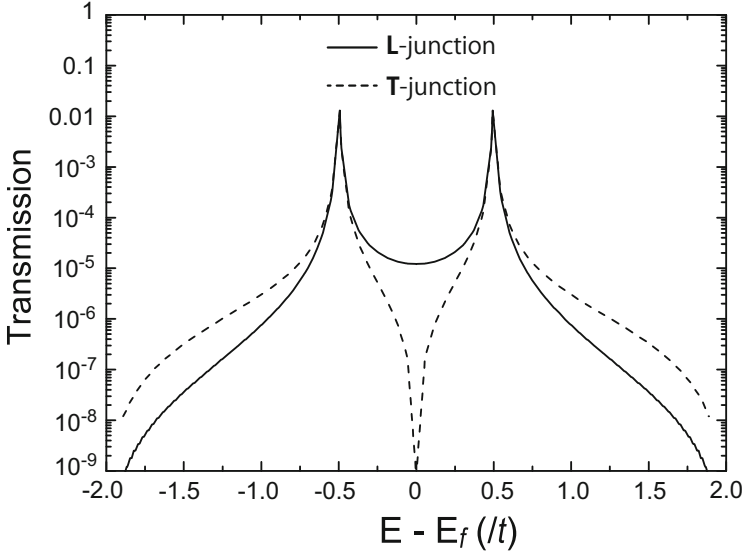
Fig. 7.4 Calculated transmission probabilities for the two contact cases, L- and T-junctions. The tight-binding parameters used in these calculations are $t_c = 0.1t$, $t_m = 0.5t$, and $\varepsilon_\alpha = \varepsilon_0 = 0$

difference in the transmission probabilities; the transmission of the T-junction drops sharply to zero (i.e., anti-resonance), whereas that for the L-junction has a parabolic shape without anti-resonance. Analysis of Green's function $G_{rs}(E)$ is quite useful to elucidate the clear difference in the transmission curves at the mid-gap. According to the pioneering study for electron tunneling by Caroli and co-workers [10], the Green's function $G_{rs}(E)$ is given in terms of the unperturbed Green's function $G_{rs}^{(0)}(E)$, as

$$G_{rs} = \frac{G_{rs}^{(0)}}{D},\tag{7.10}$$

where

$$D = (1 - t_c^2 G_{ss}^{(0)} g_{\text{elec}})(1 - t_c^2 G_{rr}^{(0)} g_{\text{elec}}) - t_c^4 G_{rs}^{(0)} G_{sr}^{(0)} g_{\text{elec}} g_{\text{elec}}.\tag{7.11}$$

Here the notation for retarded/advanced and the energy E is left off for simplicity. To derive a qualitative relationship between the orbitals and conductance, a weak coupling condition between the electrodes and sandwiched molecule is convenient; therefore, a weak coupling case was adopted in this section (i.e., the hopping parameter t_c between electrodes and a molecule is small with respect to t_m and t). According to Eq. 7.11, the renormalization term D in the weak coupling case can be clearly approximated as 1. The calculated renormalization term D for the T-junction is shown in Fig. 7.5. In weak coupling cases (i.e., smaller t_c than t), the
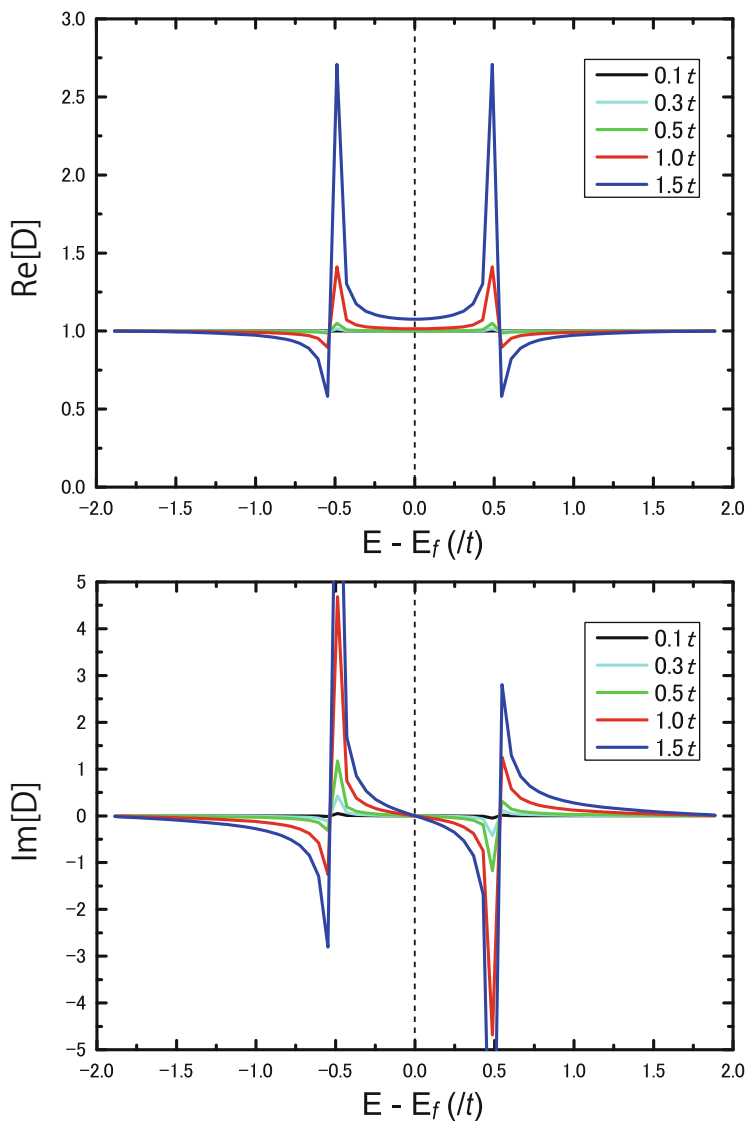
Fig. 7.5 Calculated real (Re) and imaginary (Im) parts of the renormalization term D for the T-junction. Electrode-molecule coupling t_c of 0.1, 0.3, and 0.5t are adopted as weak coupling cases, and t_c of 1.0 and 1.5t are adopted as strong coupling cases. Other TB parameters are the same as those used in the transmission calculation for the T-junction

real part of the renormalization term D (Re[D]) is almost equal to 1 at any energy; although some peaks and dips are confirmed at around eigenlevels ($-0.5t$ and $0.5t$), Re[D] at the mid-gap is apparently close to 1. In addition, the deviation of Re[D] from 1 at the mid-gap is not so large, even for strong coupling cases (i.e., larger t_c

than t), and the imaginary part of D is perfectly zero at the mid-gap, regardless of the strength of the electrode-molecule coupling t_c. We therefore unambiguously use the unperturbed Green's function $G^{(0)}$ instead of the perturbed Green's function G to figure out the relationship between the Green's function and transmission function.

We are interested in the electronic states of molecules in terms of eigenlevels (e.g., molecular orbitals of molecules); therefore, the following unperturbed Green's function expanded in terms of molecular orbitals is quite efficient:

$$G_{rs}^{(0)}(E) = \sum_k \frac{C_{rk}C_{sk}}{E - \varepsilon_k}, \qquad (7.12)$$

where the k-th eigenvalue of the isolated molecule is ε_k, and its eigenvector (i.e., orbital coefficient) on the site r is C_{rk}. Here the orbital representation of Eq. 7.12 is valid because the coefficients $C's$ of the molecule are real numbers. At the mid-gap between the HOMO and LUMO of the molecule, the contributions from the HOMO and LUMO in the summation of Eq. 7.12 are clearly significant. In the present two-site model, this situation is exactly true because we have only the two MOs, HOMO, and LUMO, and we have confirmed that the assumption also works quite well for multi-orbital systems, even with degenerate orbitals [11].

Let us consider the relationship between the MOs and Green's function. The energy differences $E - \varepsilon_k$ appear in the denominator and the orbital coefficients in the numerator in $G^{(0)}$; therefore, we can readily derive the following orbital relation for electron transport [7]: (i) large orbital coefficients at the contact sites, C_{rk} and C_{sk} for $k =$ HOMO or LUMO, lead to a large transmission probability, and (ii) opposite signs between the two terms, $C_{r\text{HOMO}}C_{s\text{HOMO}}$ and $C_{r\text{LUMO}}C_{s\text{LUMO}}$, are required for constructive interference from the HOMO and LUMO in the transmission function at the mid-gap due to the sign difference in the denominator $E - \varepsilon_k$ in $G^{(0)}$ for the HOMO and LUMO. Using the mathematical notation Sgn(a), which returns the sign of the quantity a, the second condition is written as

$$\text{Constructive(HOMO : LUMO)} : \text{Sgn}(C_{r\text{HOMO}}C_{s\text{HOMO}}C_{r\text{LUMO}}C_{s\text{LUMO}}) = -,$$
$$(7.13)$$

On the other hand, when the two terms, $C_{r\text{HOMO}}C_{s\text{HOMO}}$ and $C_{r\text{LUMO}}C_{s\text{LUMO}}$, have the same sign, the contributions from the HOMO and LUMO are canceled out at the mid-gap. In the notation using "Sgn", the relation is

$$\text{Destructive(HOMO : LUMO)} : \text{Sgn}(C_{r\text{HOMO}}C_{s\text{HOMO}}C_{r\text{LUMO}}C_{s\text{LUMO}}) = +.$$
$$(7.14)$$

Although we have focused on the HOMO and LUMO in Eqs. 7.13 and 7.14 as a frontier orbital rule for electron transport, the interference relationship between two neighboring energetically non-degenerate orbitals ε_k and ε_{k+1} can be represented as

$$\text{Constructive}(k : k + 1) : \text{Sgn}(C_{rk}C_{sk}C_{rk+1}C_{sk+1}) = -, \qquad (7.15)$$

$$\text{Destructive}(k : k + 1) : \text{Sgn}(C_{rk}C_{sk}C_{rk+1}C_{sk+1}) = +. \qquad (7.16)$$
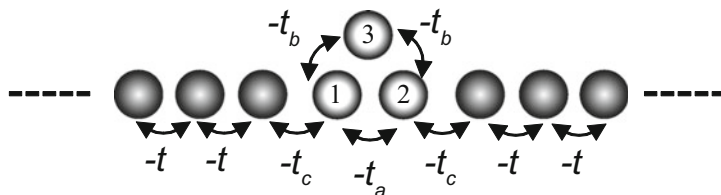
Fig. 7.6 Orbital phases of the HOMO and LUMO for the two-site molecule. The *black* and *white symbols* represent positive and negative coefficients, respectively
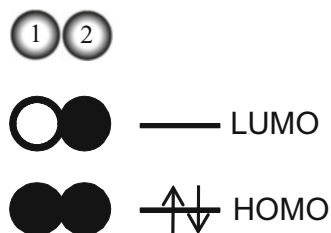
According to the orbital rule, the clear difference of the transmission functions at the mid-gap in L- and T-junctions can be readily understood. The orbital phases (i.e., the sign of MOs) of the HOMO and LUMO of the two-site molecule are shown in Fig. 7.6. In this model, the amplitude of the orbital coefficients is $1/\sqrt{2}$ for both sites. Thus, the orbital rule to consider is rule (ii). In the L-junction, the sites connected to the electrodes are sites 1 and 2. The numerator in $G^{(0)}$ for HOMO, $C_{1HOMO}C_{2HOMO}$, is a positive number, but for the LUMO, $C_{1LUMO}C_{2LUMO}$ is a negative number. This is the case for constructive interference of the electron transmission at the Fermi level, which leads to the parabolic transmission at the Fermi level without anti-resonance, as shown in Fig. 7.4. However, in the T-junction, the only site connected to the electrodes is site 1, and the terms $C_{1HOMO}C_{1HOMO}$ and $C_{1LUMO}C_{1LUMO}$ have the same sign (i.e., positive) and the same value. Therefore, the unperturbed Green's function $G^{(0)}$ at the Fermi level for the T-junction is exactly zero, which results in the sharp drop of the transmission function at the Fermi level, as shown in Fig. 7.4. This is the molecular orbital rule available for the understanding of electron transport. Application of the orbital rules for electron transport in more complicated molecules can be found elsewhere [7, 12–26].

7.2.2 Three-Site (Triangular) Model

Figure 7.7 shows Λ- and V-junctions adopted as typical three-site TB junctions, in which only a single site is connected with the left/right electrode. Figure 7.8 shows the calculated transmission functions for the Λ- and V-junctions. There are two peaks of transmission in both junctions that correspond to the eigenlevels of the triangular molecule shown in Fig. 7.9 (i.e., $-1.0t$ and $0.5t$). When the triangular system is regarded as a planar π-molecule, the molecule has three π-electrons, and the HOMO is the degenerate ε_2 or ε_3. In that sense, the mid-gap position must be recognized at the degenerate orbital level ($0.5t$), but no pronounced feature appears at this position, just a single transmission peak. On the other hand, transmission functions between $-1.0t$ and $0.5t$ show a clear difference between the Λ- and V-junctions; the Λ-junction shows a parabolic transmission, whereas the V-junction shows a sharp drop (i.e., anti-resonance) of transmission at $-0.5t$. The V-junction has only one site for coupling with the electrodes (i.e., site 3); therefore, the same explanation for the sharp drop in the T-junction also holds for the V-junction. On
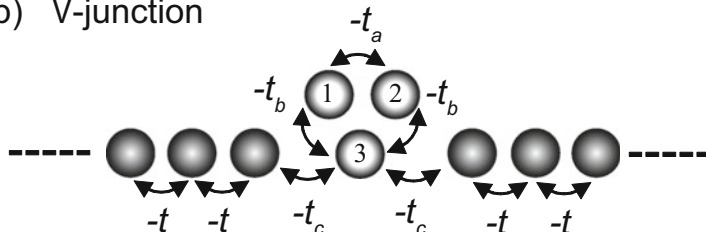
Fig. 7.7 1D tight-binding molecular junctions for the three-site triangular model. The sandwiched triangular molecule is composed of atoms 1, 2, and 3. $-t$ in the electrode, $-t_c$ for electrode-molecule hopping, and $-t_a$ and $-t_b$ for intramolecular hopping were adopted as the nearest-neighbor hopping parameters. Atoms 1 and 2 are respectively connected to the left- and right-electrodes in (**a**) the Λ-junction, and only atom 3 is connected to both electrodes in (**b**) the V-junction

the other hand, the orbital pairs of focus in the Λ- junction are $(\varepsilon_1, \varepsilon_2)$ and $(\varepsilon_1, \varepsilon_3)$. Considering the orbital phases of ε_1, ε_2, and ε_3, the pair of $(\varepsilon_1, \varepsilon_2)$ is a constructive type of interference, whereas the pair of $(\varepsilon_1, \varepsilon_3)$ represents destructive interference. However, according to the additive property in the Green's function of Eq. 7.12, a parabolic transmission from the constructive interference remains. In this sense, observation of the sharp drop of transmission (anti-resonance) is more difficult than that of the parabolic type of transmission.

Using the three-site triangular system, let us consider an orbital engineering for electron transport. Figure 7.10a shows the triangular system with three-fold rotational symmetry identical to the sandwiched molecule in Figs. 7.7, 7.8, and 7.9; the system is renamed as Λ_s. When the on-site parameters are changed depending on the atoms (e.g., the on-site parameters of atoms 1 and 2 are changed to negative and that of atom 3 to positive), the three-fold rotational symmetry is easily broken, and thus, the orbital degeneracy for ε_2 and ε_3 is also broken, which leads to three different energy levels, the Λ_a-junction in Fig. 7.10b. In the Λ-junction (i.e., the connecting atoms are 1 and 2), the orbital relationship between ε_1 and ε_2 corresponds to the *constructive* case, and that between ε_2 and ε_3 is also *constructive*. Thus, the calculated transmission function shows parabolic transmission in both the $(\varepsilon_1 : \varepsilon_2)$ and $(\varepsilon_2 : \varepsilon_3)$ regions, as shown in Fig. 7.11. When the base of the Hamiltonian matrix of the triangular system is π-AO, the system corresponds exactly to a
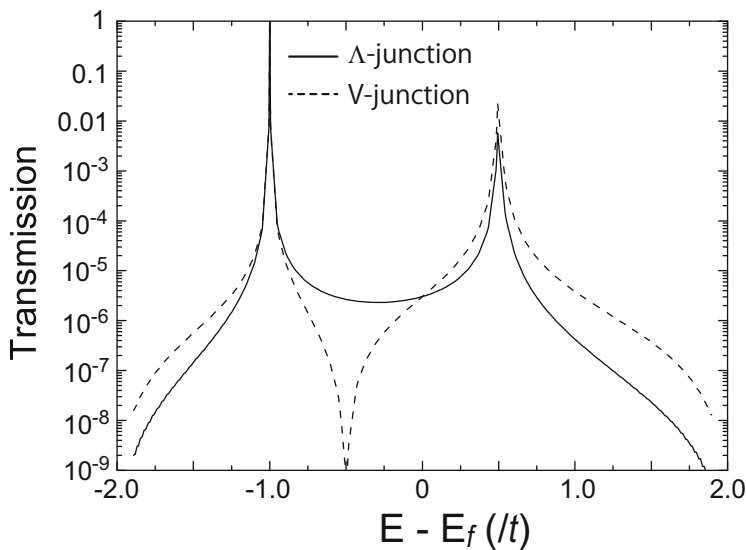
Fig. 7.8 Calculated transmission probabilities for the three-site models, Λ- and V-junctions. The tight-binding parameters used in the calculations are $t_c = 0.1t$, $t_a = t_b = 0.5t$, and $\varepsilon_\alpha = \varepsilon_0 = 0$
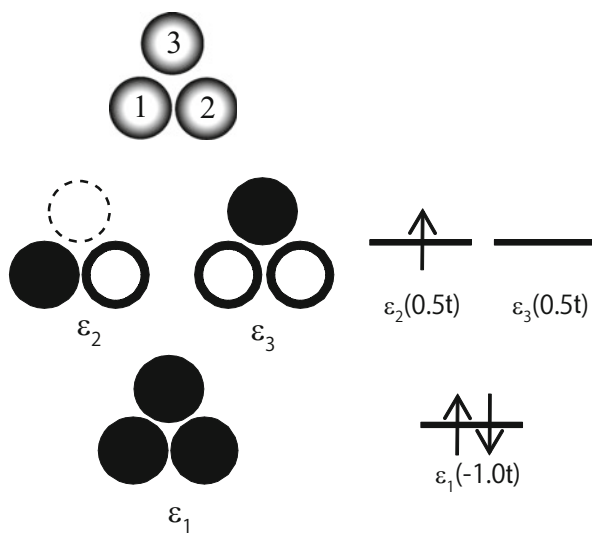

Fig. 7.9 Orbital phases of ε_1, ε_2, and ε_3 for the three-site triangular molecule. The *black* and *white symbols* represent positive and negative coefficients, respectively. The *dotted circle indicates* the zero orbital amplitude
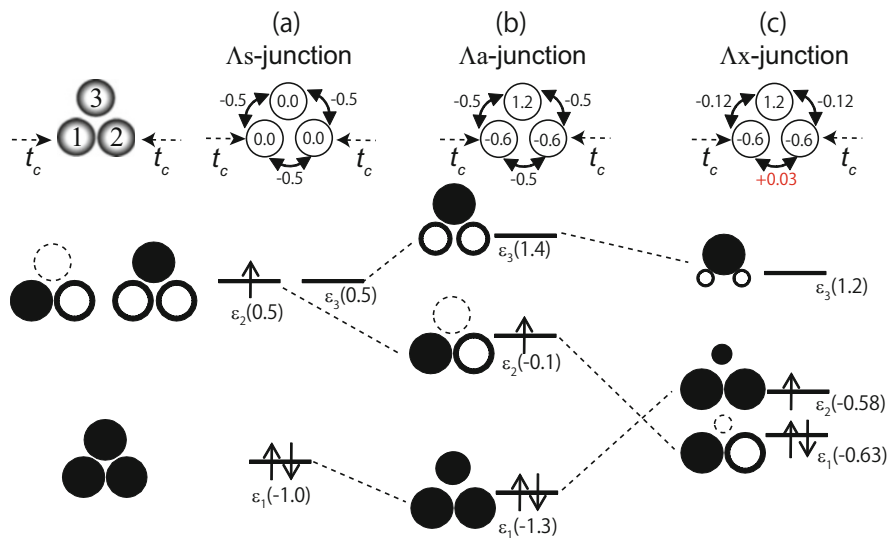
Fig. 7.10 Orbital schematics for orbital engineering in the triangular system. (**a**) Λ_s junction: TB parameters maintain the threefold rotational symmetry, and this junction is identical to the original triangular junction in Fig. 7.9. (**b**) Λ_a junction: the threefold rotational symmetry is broken by changing the on-site parameters. (**c**) Λ_x junction: the sign of the hopping parameter in Λ_a junction is changed from negative to positive (*red*). The *dotted circles* represent the zero orbital amplitudes

planar triangular molecule, and thus the intramolecular hopping parameter (i.e., $-t_a$ and $-t_b$) is a negative value because of the $\pi - \pi$ orbital interactions. Thus, the resultant transmission functions in the triangular molecular system have basically the same features as the transmission functions of the Λ_s- and Λ_a-junctions shown in Fig. 7.11.

However, when the Hamiltonian matrix is given as an MO base, the hopping parameters between the neighboring sites (MOs) can be both positive and negative, whereby an intrinsically different transmission appears, compared with those of the Λ_s- and Λ_a-junctions. When the hopping parameter between sites 1 and 2 is changed to a positive number, the orbital order for ε_1 and ε_2 in the Λ_s- and Λ_a-junctions can be exchanged, as shown in Fig. 7.10c, Λ_x-junction. As a result of the orbital order exchange in the Λ_x-junction, the orbital relationship between ε_2 and ε_3 becomes *destructive*, and a clear drop of transmission appears in between the orbital ε_2 and ε_3 (i.e., $-0.58t$ and $1.2t$), as shown in Fig. 7.11. In this way, orbital engineering based on the orbital rule for electron transport is useful to predict the qualitative properties of transport.
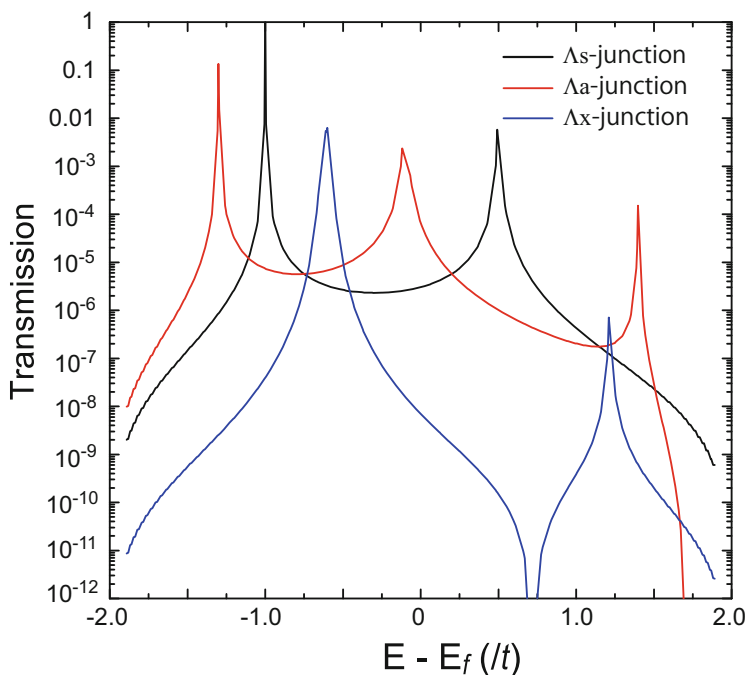
Fig. 7.11 Calculated transmission probabilities for the Λ_s, Λ_a, and Λ_x junctions. The tight-binding parameters used in the calculations are given in Fig. 7.10

7.2.3   *Orbital Rule from Experimental Observations*

Now that the relationship between orbitals and transmission functions from a theoretical perspective is explained, the next concern is the experimental validation of the orbital rule. In the experimental observation of electron transport in molecular junctions, sulfur atoms are typically introduced as an alligator clip with gold electrodes because Au-S bonding is sufficiently strong (strong coupling) to trap a single molecule between electrodes; dithiolate molecules are frequently adopted to make single molecular junctions. Therefore, whether the orbital rule using the simplest TB model can be applicable to such realistic Au-dithiole-Au junctions must be discussed first. As for this point, basic analysis and more sophisticated calculations based on density functional theory (DFT) for electron transport have been successful for validation of the orbital rules [25]. In addition, analysis of the renormalization term D in a strong coupling case, as shown in Fig. 7.5, supports the applicability of the orbital rule derived in a weak coupling case.

Let's move on to the experimental observations related to the orbital rule. The direct observation of the transmission function requires a more careful handling of junctions than in current measurements; therefore, the electrical current would be an easier quantity available for such validation. In fact, validation of the orbital

rule was performed based on the observed current first, and validation using the observed transmission (i.e., derivative conductance) was then accomplished. The first experimental validation was conducted by Taniguchi and co-workers [27], in which naphthalenedithiole (ND) molecules were adopted in current measurements. In the experimental work, four ND molecules, shown in Fig. 7.12a, were synthesized, and the tunneling current of the junctions using gold electrodes was calculated and measured. According to the orbital phases of the ND molecules (Fig. 7.12a), four molecules appear to have the constructive pattern of MOs at first inspection; however, 2,7-ND is the exception because only 2,7-ND has two singly-occupied MOs (SOMOs), i.e., a case of degenerate frontier MOs. The two SOMO can be transformed into another two pairs of MOs by unitary transformation, and the resultant MOs can be perfectly localized frontier MOs, left-edge localized MO and right-edge localized MO. Orbital rule I for electron transport tells us that non-zero orbital amplitudes at the connecting atoms are required in frontier orbitals. Therefore, the zero amplitudes at the connecting atoms cannot be used for transport, and 2,7-ND is an undesirable molecule in terms of the orbital amplitudes, which results in extremely low transmission (Fig. 7.12b). The details of the orbital rule for the degenerate case, which is not addressed in the chapter, has been described in a recent work using a benzene molecular junction [11]. Figure 7.12c shows the clear correspondence with the theoretical predictions based on the orbital rule.

After the experiment using ND molecules, Guédon and co-workers accomplished more direct observations of *constructive/destructive* interference [28] using the anthraquinone molecular unit shown in Fig. 7.13. According to their explanation, the anthraquinone molecular unit can be regarded as a three-site model, in which the interorbital interactions correspond to the Λ_x triangular system shown in Fig. 7.10c.[2] Therefore, *destructive* interference is expected to appear in the molecular junction, and a sharp drop of the transmission function at the Fermi level was actually observed. In this way, the validity of the orbital rule was successfully confirmed from indirect/direct measurements of the transmission probabilities in molecular junctions.

7.2.4 Spin-Dependent Transport in Molecular Spin Junctions

In this section, we discuss the applicability of the orbital rule for spin-dependent transport. When a sandwiched molecule has a localized spin and the molecular-spin junction shows a spin-dependent transport without spin-flip processes, the orbital rule introduced in the previous part is straightforwardly applicable for the

---

[2]According to their three-site model, the hopping parameters between sites 1 and 3 (2 and 3) are also positive, whereas Λ_x-junction is negative for these. However, it was confirmed that the intrinsic property (anti-resonance) in the Λ_x-junction was not sensitive to the sign of the 1–3 and 2–3 hopping parameters. The key parameter for the anti-resonance is the sign for hopping between sites 1 and 2 because the key factor is the orbital exchange between ε_1 and ε_2 from Λ_a to Λ_x
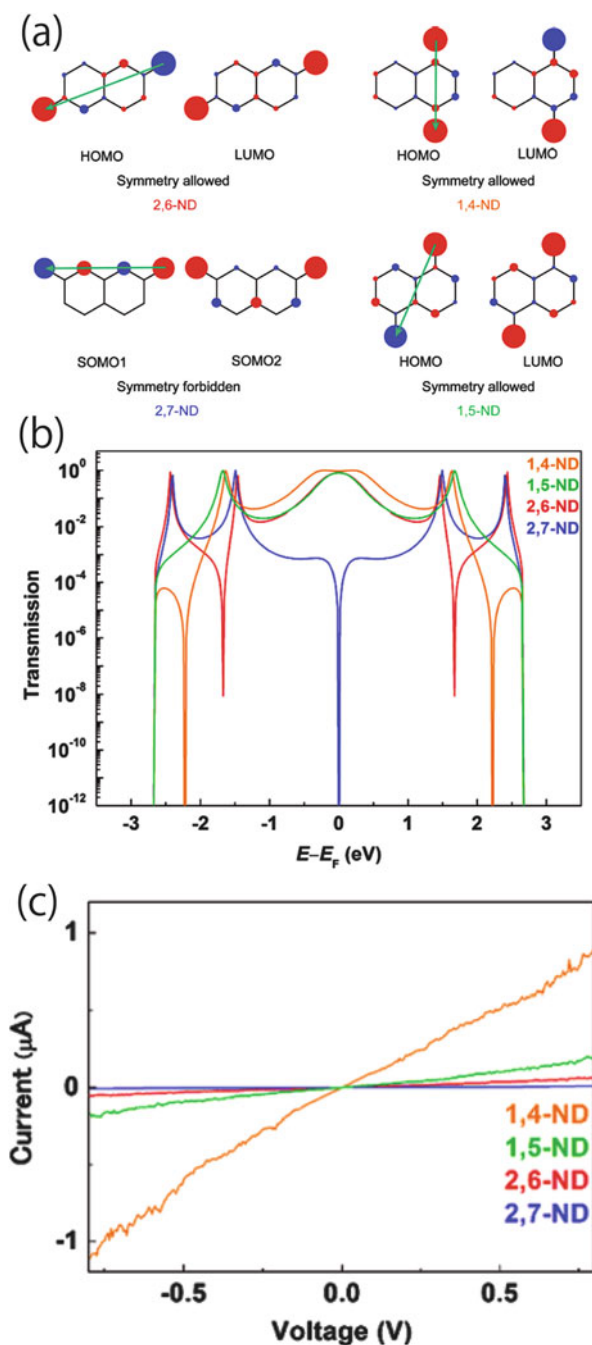
Fig. 7.12 (**a**) Naphthalene dithiolate (ND) molecules, (**b**) calculated transmission functions of the ND molecules, and (**c**) measured current reported by Taniguchi and co-workers (Reprinted with permission from Ref. [27]. Copyright 2011 American Chemical Society)
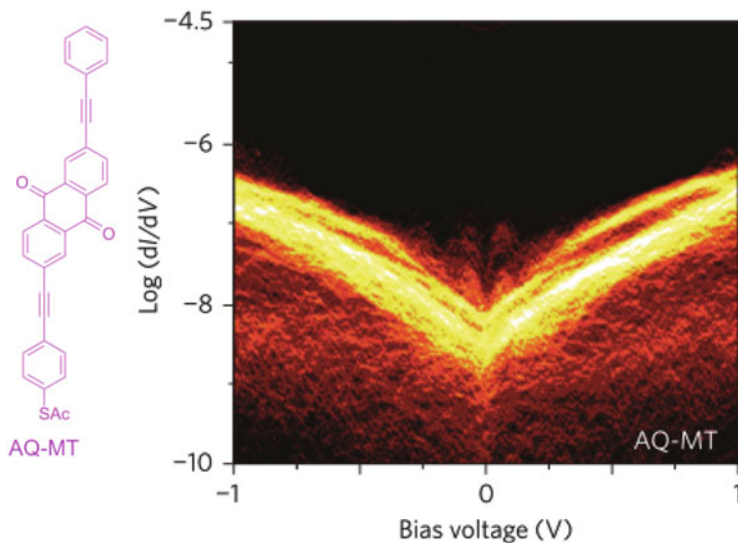
Fig. 7.13 Anthraquinone molecular unit showing an anti-resonance transmission of the Fermi level, and the measured transmission function (i.e., derivative conductance) by Guédon and co-workers (Reprinted with permission from Ref. [28]. Copyright 2012 Nature Publishing Group)
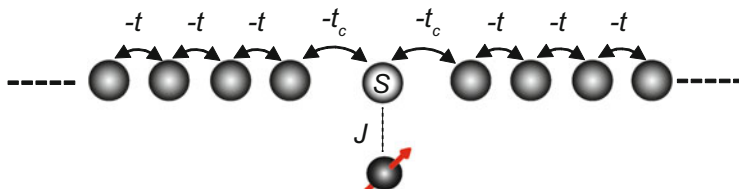

Fig. 7.14 Tight-binding 1D model including a localized electron spin. The gray atom (or molecule) indexed with s is coupled to electrodes and to a localized spin (*red*) through the spin-spin exchange coupling, J. The nearest-neighbor hopping integrals are represented by t and t_c

spin-dependent transport because the matrix elements for each spin can be written independently. Thus, we can discuss the transmission properties in both spin cases (e.g., up- or down-spin) separately. However, when spin-flip processes are allowed by the spin exchange coupling between a conduction electron and localized spin, the matrix elements are not divided into submatrices in terms of up- or down-spin. For example, the 1D system shown in Fig. 7.14 corresponds to such a spin system,

and the Hamiltonian matrix is written as

$$
\mathbf{H_{spin}} =
\begin{array}{c}
\\
s{-}2_{\downarrow} \\
s{-}1_{\uparrow} \\
s{-}1_{\downarrow} \\
s_{\uparrow\Downarrow} \\
s_{\downarrow\Uparrow} \\
s{+}1_{\uparrow} \\
s{+}1_{\downarrow} \\
s{+}2_{\uparrow}
\end{array}
\begin{array}{c}
\begin{array}{cccccccc}
s{-}2_{\downarrow} & s{-}1_{\uparrow} & s{-}1_{\downarrow} & s_{\uparrow\Downarrow} & s_{\downarrow\Uparrow} & s{+}1_{\uparrow} & s{+}1_{\downarrow} & s{+}2_{\uparrow}
\end{array} \\
\left(
\begin{array}{cccccccc}
\varepsilon_0 & 0 & -t & & & & & \\
0 & \varepsilon_0 & 0 & -t_c & & & & \\
-t & 0 & \varepsilon_0 & 0 & -t_c & & & \\
 & -t_c & 0 & \frac{-J}{4} & \frac{J}{2} & -t_c & & \\
 & & -t_c & \frac{J}{2} & \frac{-J}{4} & 0 & -t_c & \\
 & & & -t_c & 0 & \varepsilon_0 & 0 & -t \\
 & & & & -t_c & 0 & \varepsilon_0 & 0 \\
 & & & & & -t & 0 & \varepsilon_0
\end{array}
\right),
\end{array}
$$

$$(7.17)$$

where $\uparrow$ and $\downarrow$ are the spin directions of conduction electrons and $\Uparrow$ and $\Downarrow$ are the spin directions of the localized spin (red arrow in Fig. 7.14). The spin exchange coupling J, between the conduction and localized electron spins, was taken into account through the s-d tight-binding Hamiltonian in Eq. 7.17. In this sense, the spin-junction is a mimic of an aromatic molecule including a d-metal center, such as the metal-phthalocyanine molecular junction with gold chains fabricated by Nazin and co-workers (see Fig. 7.15) [29]. The presence of the spin-spin coupling term $J/2$ with the matrix elements $(s_{\uparrow\Downarrow}, s_{\downarrow\Uparrow})$ and $(s_{\downarrow\Uparrow}, s_{\uparrow\Downarrow})$ of $\mathbf{H_{spin}}$ means that the incoming up-spin electron can be transmitted/reflected as up- or down-spin; the same situation is also observed for the incoming down-spin. Thus, the Hamiltonian $\mathbf{H_{spin}}$ cannot be divided into spin-dependent Hamiltonians. In this case, a straightforward method for the transport calculation is a wave-packet propagation; the simulation is useful to calculate the transport processes including spin-flip, and multiple spin-flip processes can also occur at the spin site s, which corresponds to incoherent transport. Although the wave-packet propagation method is a very useful method, the calculation for the transmission curves from wave-packet dynamics requires numerical propagations of the wave-packet for each energy level, and thus it could be time consuming, depending on the system size and the required energy width and resolution. Therefore, if the Green's function method is also applicable for the present spin-flip case, then it would be better to use it.

7.2.4.1 Coherent Approach for the Spin-Flip Process

For the Green's function approach, the first step is a division of the entire process into coherent and incoherent processes because the transport process including spin-flip is a mixture of coherent and incoherent processes. Let us consider a simple
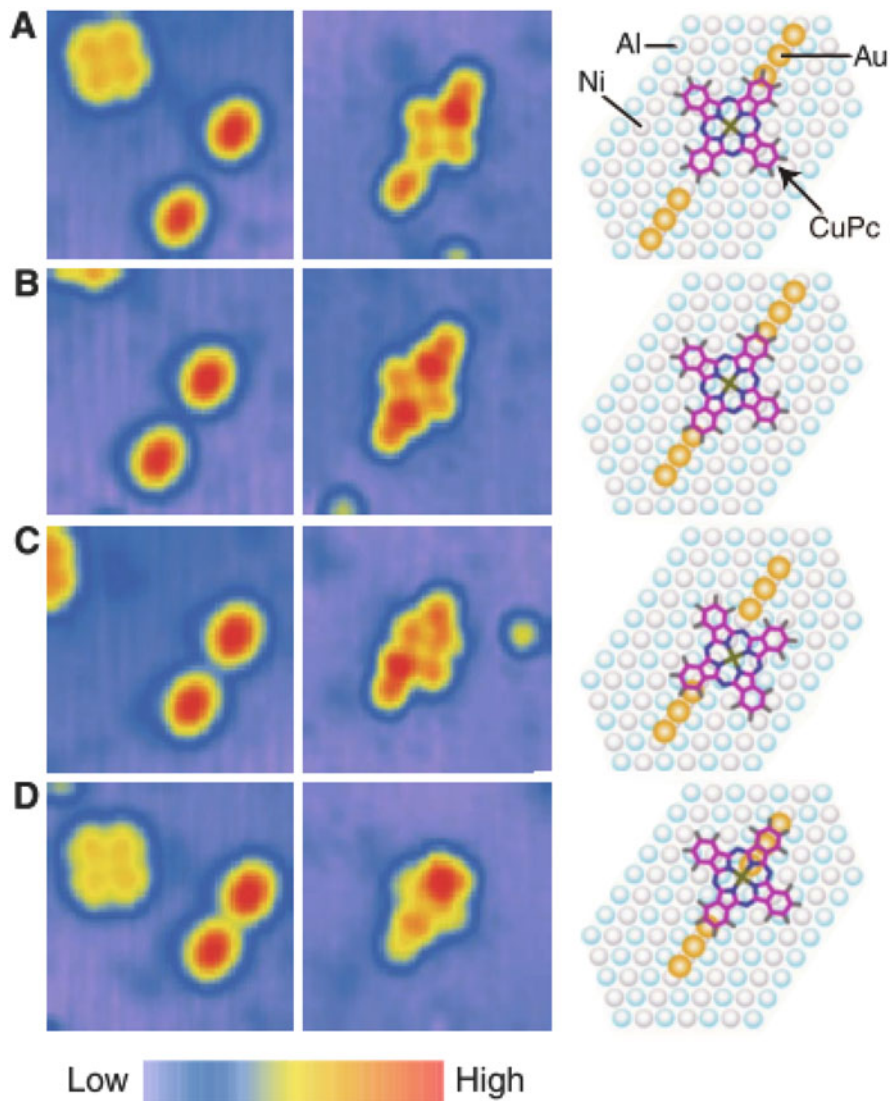
Fig. 7.15 Scanning tunneling microscopy (STM) image of a gold-Cu phthalocyanine-gold junction on a NiAl substrate taken by Nazin, Qiu, and Ho (Reprinted with permission from Ref. [29]. Copyright 2003 AAAS)

case, in which the incoming electron is initially spin polarized as up-spin. Under this condition, there are two coherent processes:

[Spin-Flip case:] $\cdots \uparrow_{s-2} \rightarrow \uparrow_{s-1} \rightarrow \uparrow_s \rightarrow \downarrow_s \rightarrow \downarrow_{s+1} \rightarrow \downarrow_{s+2} \cdots$
[No Flip case:] $\cdots \uparrow_{s-2} \rightarrow \uparrow_{s-1} \rightarrow \uparrow_s \rightarrow \uparrow_{s+1} \rightarrow \uparrow_{s+2} \cdots.$

The corresponding submatrices for the spin-flip (SF) and no-flip (NF) processes are respectively given as

$$
\mathbf{H}_{s\uparrow-\downarrow}^{(SF)} =
\begin{array}{c}
\\
\vdots \\
s-2_\uparrow \\
s-1_\uparrow \\
s_{\uparrow\Downarrow} \\
s_{\downarrow\Uparrow} \\
s+1_\downarrow \\
s+2_\downarrow \\
\vdots
\end{array}
\begin{array}{c}
\begin{array}{ccccccc}
\cdots & s-2_\uparrow & s-1_\uparrow & s_{\uparrow\Downarrow} & s_{\downarrow\Uparrow} & s+1_\downarrow & s+2_\downarrow & \cdots
\end{array} \\
\left(
\begin{array}{ccccccc}
\ddots & \ddots & & & & & \\
\ddots & \varepsilon_0 & -t & & & & \\
 & -t & \varepsilon_0 & -t_c & & & \\
 & & -t_c & \frac{-J}{4} & \frac{J}{2} & 0 & \\
 & & & \frac{J}{2} & \frac{-J}{4} & -t_c & \\
 & & & 0 & -t_c & \varepsilon_0 & -t \\
 & & & & & -t & \varepsilon_0 & \ddots \\
 & & & & & & \ddots & \ddots
\end{array}
\right),
\end{array}
$$

(7.18)

and

$$
\mathbf{H}_{s\uparrow-\uparrow}^{(NF)} =
\begin{array}{c}
\\
\vdots \\
s-2_\uparrow \\
s-1_\uparrow \\
s_{\uparrow\Downarrow} \\
s_{\downarrow\Uparrow} \\
s+1_\uparrow \\
s+2_\uparrow \\
\vdots
\end{array}
\begin{array}{c}
\begin{array}{ccccccc}
\cdots & s-2_\uparrow & s-1_\uparrow & s_{\uparrow\Downarrow} & s_{\downarrow\Uparrow} & s+1_\uparrow & s+2_\uparrow & \cdots
\end{array} \\
\left(
\begin{array}{ccccccc}
\ddots & \ddots & & & & & \\
\ddots & \varepsilon_0 & -t & & & & \\
 & -t & \varepsilon_0 & -t_c & & & \\
 & & -t_c & \frac{-J}{4} & \frac{J}{2} & -t_c & \\
 & & & \frac{J}{2} & \frac{-J}{4} & 0 & \\
 & & & -t_c & 0 & \varepsilon_0 & -t \\
 & & & & & -t & \varepsilon_0 & \ddots \\
 & & & & & & \ddots & \ddots
\end{array}
\right).
\end{array}
$$

(7.19)

These matrices clearly have the same matrix form already introduced in the two-site TB model, L-, and T-junctions. Replacement of the tight-binding parameters ε_α in Eqs. 7.7 and 7.8 with $-J/4$ and $-t_m$ in Eqs. 7.7 and 7.8 with $J/2$ leads to the matrices $\mathbf{H}_{s\uparrow-\downarrow}^{(SF)}$ and $\mathbf{H}_{s\uparrow-\uparrow}^{(NF)}$ being easily determined as exactly equal to $\mathbf{H_L}$ and $\mathbf{H_T}$, respectively. Therefore, the coherent spin-flip process corresponds to *constructive* transport, and the coherent no-flip process corresponds to *destructive* transport. We can understand the validity of the consideration in another point of view as follows. As for the coherent no-flip process, the Hamiltonian matrix can be expressed in a spin-dependent form because spin-exchange does not occur, and the junction structure in Fig. 7.14 is the same as that of the T-junction where a single atom is connected to both electrodes. Therefore, *destructive* transport must appear in the no-flip transport of the junction in Fig. 7.14.

Figure 7.16 shows the calculated transmission probabilities for the $\uparrow$-to-$\uparrow$ and $\uparrow$-to-$\downarrow$ processes using the matrices of Eqs. 7.18 and 7.19. The eigenlevels of the spin junction system are $-0.15t$ singlet state, and $0.05t$ triplet state ($0.2t$ of J
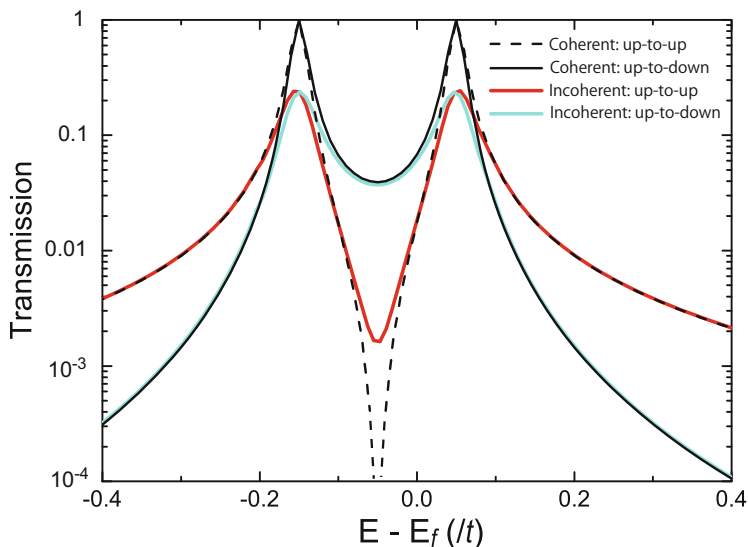
Fig. 7.16 Calculated transmission probabilities for the ↑-to-↑ and ↑-to-↓ processes with the coherent two-probes Green's function and incoherent four-probes Green's function approaches. The tight-binding parameters adopted in the calculations are $0.1t$ of t_c and $0.2t$ of J

was used in Fig. 7.16); therefore, two transmission peaks appear at the positions in both processes. As expected in the matrix forms, the spin-flip process shows a parabolic transmission between the two peaks, and the no-flip process shows a clear drop at the mid-gap of the two eigenlevels. This confirms that the process-dependent matrix division is a useful way to understand the intrinsic transport properties (i.e., *constructive* or *destructive*). The next point to be considered is the influence of the incoherent processes that are neglected in the previous framework. In order to discuss this point, the differences between the results from the Green's function based only on coherent processes and wave-packet propagation have to be recognized, and the relationship between the results from the wave-packet method and Green's function including incoherent processes has to be discussed. These comparisons were made in the previous study [24], and excellent correspondence between the Green's function with incoherent processes and the wave-packet method was confirmed. Therefore, in the next section, the Green's function including incoherent processes is introduced. The simulations for charge transport using wave-packet dynamics can be found in applications for organic molecular systems [30–33].

7.2.4.2   Incoherent Approach for the Spin-Flip Process

The coherent approximation made in the previous part includes a clear shortcoming in that the division of the entire process into ↑-to-↓ and ↑-to-↑ processes eliminates the interference between the two processes. Thus, the missing processes in the coherent ↑-to-↓ are i) the escape (transmission) of an electron with up-spin at site s to the right-electrode $s + 1$ with the same spin, and ii) the reflection back effect of this process into the ↑-to-↑ process. This is related to the hopping integrals $-t_c$ at $(s_{\uparrow\Downarrow}, s+1_\uparrow)$ and $(s+1_\uparrow, s_{\uparrow\Downarrow})$ of $\mathbf{H_{spin}}$, which are neglected in $\mathbf{H^{(SF)}_{s\uparrow-\downarrow}}$. To take the missing effects into account in the Green's function approach, an excess probe can be introduced using an appropriate self-energy [8]. The incoherent effect to be included is the interaction $-t_c$ between site s and the right electrode site $s+1$ with the same spin; therefore, the 2×2 self-energy matrix can be written as

$$(\Sigma^s_{s\uparrow\Downarrow})_{i,j} = t_c^2 g_{\text{elec}} \delta_{ij} \delta_{i1}. \tag{7.20}$$

Similarly, the missing processes in the coherent ↑-to-↑ are iii) the escape (transmission) of an electron with down-spin at site s to the right-electrode $s + 1$ with the same down-spin, and iv) the reflection back effect of this process into the ↑-to-↓ process. This is related to the hopping integrals $-t_c$ at $(s_{\downarrow\Uparrow}, s+1_\downarrow)$ and $(s+1_\downarrow, s_{\downarrow\Uparrow})$ of $\mathbf{H_{spin}}$, which are neglected in $\mathbf{H^{(NF)}_{s\uparrow-\uparrow}}$. The related 2×2 self-energy matrix is[3]:

$$(\Sigma^s_{s\downarrow\Uparrow})_{i,j} = t_c^2 g_{\text{elec}} \delta_{ij} \delta_{i2}. \tag{7.21}$$

Therefore, the Green's function including the incoherent processes (i.e., the four-probe Green's function) can be written as

$$\mathbf{G}^{A/R}_4(E) = [E\mathbf{1} - \mathbf{H^{(s1)}} - \Sigma^{A/R}_L - \Sigma^{A/R}_R - \Sigma^{s,A/R}_{s\uparrow\Downarrow} - \Sigma^{s,A/R}_{s\downarrow\Uparrow}]^{-1}, \tag{7.22}$$

where $\mathbf{H^{(s1)}}$ is the 2×2 matrix at site s ($s_{\uparrow\Downarrow}$ and $s_{\downarrow\Uparrow}$) in Eqs. 7.18 and 7.19.

The solid blue and red lines in Fig. 7.16 are the calculated transmission functions using the four-probe Green's function, which show almost perfect correspondence with the results obtained with the WP dynamics (not shown). The peak height at the resonance position (i.e., eigenlevels) is slightly decreased as a result of the additional escape processes (incoherent processes). In addition, the anti-resonance observed in the coherent no-flip process is slightly weakened, although it is still recognizable. Thus, the coherent approximation is confirmed as reasonable to capture the transport properties qualitatively, and a quantitative description for the incoherent processes is possible using the Green's function including additional appropriate self-energies.

---

[3]The explanations for the neglected incoherent processes given in this part are originally from Ref. [24]. However, there is a typographical error in Eq. (21) of Ref. [24]; the equations shown here in this section are correct.

7.3 Summary

In this chapter, the orbital rule (or HOMO-LUMO rule) to achieve a qualitative understanding of electron transport in molecular junctions was introduced on the basis of the Green's function method. There is no limitation in the orbital basis used for the orbital rule; AOs, MOs, and spin-spin direct product bases are available for an understanding of the *constructive* and *destructive* interference effects in electron transport. In the AO picture, the two-site tight-binding model was adopted to determine the key factor in *constructive* and *destructive* interference. This model is a minimum model because only the HOMO and LUMO appear as the orbital levels of the two-site model. Many examples of the orbital rule applied to other large molecules (i.e., multi-orbital systems) can be found in the literature; for example, nanographite with armchair and zigzag edges [7, 12, 14], DNA molecules [13], aromatic dithiolate molecules [16], metal-phthalocyanine molecules [17], photochromic molecules [18], and π-stacked molecules [11, 34–37]. In a recent work, a concept for a conductance decay-free junction was derived from the orbital rule. In the molecular orbital picture, the triangular three-site model was used to explain the observed *destructive* interference of an anthraquinone molecular unit in a recent experiment. The key is the orbital-phase exchange that originates from the sign-change of the hopping parameters between neighboring sites.

In the final part of this chapter, the *spin-flip transport* in a simple 1D tight-binding chain including a localized spin was discussed using the Green's function with and without incoherent spin-flip processes on the basis of the spin-spin direct product base. The spin exchange coupling J, between the conduction and localized electron spins, was taken into account through the s-d tight-binding Hamiltonian. In this sense, the spin-junction is a mimic of an aromatic molecule that includes a d-metal center. The transmission probabilities that depend on the spin directions at the drain electrode were analyzed; the $\uparrow$-to-$\uparrow$ process for the incoming up-spin is transmitted as the outgoing up-spin, and the $\uparrow$-to-$\downarrow$ process for the incoming up-spin is transmitted as the outgoing down-spin. The Green's function calculations show that the transmission probabilities for both processes have large peaks at the eigenlevels of the spin singlet ($-3J/4$) and triplet ($J/4$) states and that the transmission probabilities exhibit different properties, depending on the spin-flip processes at the mid-gap (anti-resonance level) of the two eigenlevels; the $\uparrow$-to-$\uparrow$ process shows an abrupt drop, whereas the $\uparrow$-to-$\downarrow$ process shows a parabolic transmission. The similarity of the matrix forms for $\uparrow$-to-$\downarrow$ transport and a two-site constructive junction (i.e., L-junction) was easily confirmed with reference to the orbital rule for coherent electron transport in a molecular junction; the similarity between $\uparrow$-to-$\uparrow$ transport and a two-site destructive junction (i.e., T-junction) was also recognized.

It should be emphasized that the orbital rule is a qualitative rule for the understanding of transport properties; however, the concepts derived from the rule will lead to a wide range of applications for molecular- and nanojunctions.

References

 1. Aharonov Y, Bohm D (1959) Significance of electromagnetic potentials in the quantum theory. Phys Rev 115:485–491
 2. Peshkin M, Tonomura A (1989) The Aharonov—Bohm effect. Springer
 3. Sautet P, Joachim C (1988) Electronic interference produced by a benzene embedded in a polyacetylene chain. Chem Phys Lett 153:511–516
 4. Kemp M, Roitberg A, Mujica V, Wanta T, Ratner M A (1996) Molecular wires: extended coupling and disorder effects. J Phys Chem 100:8349
 5. Emberly E G, Kirczenow G (1999) Antiresonances in molecular wires. J Phys: Condens Matter 11:6911
 6. Baer R, Neuhauser D (2002) Phase coherent electronics: a molecular switch based on quantum interference. J Am Chem Soc 124:4200–4201
 7. Tada T, Yoshizawa K (2002) Quantum transport effects in nanosized graphite sheets. ChemPhysChem 3:1035
 8. Datta S (1995) Electronic transport in mesoscopic systems. Cambridge University Press, Cambridge
 9. Landauer R (1957) Spatial variation of currents and fields due to localized scatterers in metallic conduction. IBM J Res Dev 1:223–231
10. Caroli C, Combescot R, Nozieres P, Saint-James D (1971) Direct calculation of the tunneling current. J Phys C 4:916
11. Tada T, Yoshizawa K (2015) Molecular design of electron transport with orbital rule: toward conductance-decay free molecular junctions. Phys Chem Chem Phys 17:32099–32110
12. Tada T, Yoshizawa K (2003) Quantum transport effects in nanosized graphite sheets. II. Enhanced transport effects by heteroatoms. J Phys Chem B 107:8789–8793
13. Tada T, Kondo M, Yoshizawa K (2003) Theoretical measurements of conductance in an (AT)12 DNA molecule. ChemPhysChem 4:1256
14. Tada T, Yoshizawa K (2004) Reverse exponential decay of electrical transmission in nanosized graphite sheets. J Phys Chem B 108:7565–7572
15. Kondo M, Tada T, Yoshizawa K (2004) Wire-length dependence of the conductance of oligo (p-phenylene) dithiolate wires: a consideration from molecular orbitals. J Phys Chem A 108:9143
16. Tada T, Nozaki D, Kondo M, Hamayama S, Yoshizawa K (2004) Oscillation of conductance in molecular junctions of carbon ladder compounds. J Am Chem Soc 126:14182
17. Tada T, Hamayama S, Kondo M, Yoshizawa K (2005) Quantum transport effects in copper (II) phthalocyanine sandwiched between gold nanoelectrodes. J Phys Chem B 109:12443
18. Kondo M, Tada T, Yoshizawa K (2005) A theoretical measurement of the quantum transport through an optical molecular switch. Chem Phys Lett 412:55
19. Yoshizawa K, Tada T, Staykov A (2008) Orbital views of the electron transport in molecular devices. J Am Chem Soc 130:9406–9413
20. Tsuji Y, Staykov A, Yoshizawa K (2009) Orbital control of the conductance photoswitching in diarylethene. J Phys Chem C 113:21477–21483

21. Li X, Staykov A, Yoshizawa K (2010) Orbital views of the electron transport through polycyclic aromatic hydrocarbons with different molecular sizes and edge type structures. J Phys Chem C 114:9997–10003
22. Li X, Staykov A, Yoshizawa K (2011) Orbital views of the electron transport through heterocyclic aromatic hydrocarbons. Theor Chem Acc 50:6200–6209
23. Tsuji Y, Staykov A, Yoshizawa K (2011) Orbital views of molecular conductance perturbed by anchor units. J Am Chem Soc 133:5955–5960
24. Tada T, Yamamoto T, Watanabe S (2011) Molecular orbital concept on spin-flip transport in molecular junctions. Theor Chem Acc 130:775–788
25. Yoshizawa K (2012) An orbital rule for electron transport in molecules. Acc Chem Res 45:1612–1621
26. Li X, Staykov A, Yoshizawa K (2012) Orbital views on electron-transport properties of cyclophanes: insight into intermolecular transport. Bull Chem Soc Jpn 85:181–188
27. Taniguchi M, Tsutsui M, Mogi R, Sugawara T, Tsuji Y, Yoshizawa K, Kawai, T (2011) Dependence of single-molecule conductance on molecule junction symmetry. J Am Chem Soc 133:11426–11429.
28. Guédon CM, Valkenier H, Markussen T, Thygesen KS, Hummelen JC, van der Molen SJ (2012) Observation of quantum interference in molecular charge transport. Nat Nanotechnol 7:305–309
29. Nazin G V, Qiu X H, Ho W (2003) Visualization and spectroscopy of a metal-molecule-metal bridge. Science 302:77
30. Troisi A, Orlandi G (2006) Charge-transport regime of crystalline organic semiconductors: diffusion limited by thermal off-diagonal electronic disorder. Phys Rev Lett 96:086601
31. Ishii H, Kobayashi N, Hirose K (2010) Order-N electron transport calculations from ballistic to diffusive regimes by a time-dependent wave-packet diffusion method: Application to transport properties of carbon nanotubes. Phys Rev B 82:085435
32. Terao J, Wadahama A, Matono A, Tada T, Watanabe S, Seki S, Fujihara T, Tsuji Y (2013) Design principle for increasing charge mobility of pi-conjugated polymers using regularly localized molecular orbitals. Nat Commun 4:1691
33. Ito Y, Takai K, Miyazaki A, Sivamurugan V, Kiguchi M, Ogawa Y, Nakamura N, Valiyaveettil S, Tada T, Watanabe S, Enoki T (2014) Anomalous metallic-like transport of Co–Pd ferromagnetic nanoparticles cross-linked with pi-conjugated molecules having a rotational degree of freedom. Phys Chem Chem Phys 16:288–296
34. Kiguchi M, Takahashi T, Takahashi Y, Yamauchi Y, Murase T, Fujita M, Tada T, Watanabe S (2011) Electron transport through single molecules comprising aromatic stacks enclosed in self-assembled cages. Angew Chem Int Ed 50:5708–5711
35. Tsuji Y, Staykov A, Yoshizawa K (2011) Molecular rectifier based on pi-pi stacked charge transfer complex. J Phys Chem C 116:2575–2580
36. Kiguchi M, Inatomi J, Takahashi Y, Tanaka R, Osuga T, Murase T, Fujita M, Tada T, Watanabe S (2013) Highly conductive $[3\times n]$ gold-ion clusters enclosed within self-assembled cages. Angew Chem Int Ed 52:6202–6205
37. Fujii S, Tada T, Komoto Y, Osuga T, Murase T, Fujita M, Kiguchi M (2015) Rectifying electron-transport properties through stacks of aromatic molecules inserted into a self-assembled cage. J Am Chem Soc 137:5939–5947